

# Instantons and the Chiral Phase Transition at non-zero Baryon Density

T. Schäfer

*Institute for Nuclear Theory, Department of Physics, University of Washington,  
Seattle, WA 98195, USA*

## Abstract

We study an interacting ensemble of instantons at finite baryon chemical potential. We emphasize the importance of fermionic zero modes and calculate the fermion induced interaction between instantons at non-zero chemical potential. We show that unquenched simulations of the instanton ensemble are feasible in two regimes, for sufficiently small and for very large chemical potential. At very large chemical potential chiral symmetry is restored and the instanton ensemble is dominated by strongly correlated chain-like configurations.

11.30.Rd, 12.38.Lg, 12.38.Mh

arXiv:hep-ph/9708256v2 17 Nov 1997

## I. INTRODUCTION

The behavior of matter under extreme conditions of temperature and/or density is of great interest in connection with the physics of heavy ion collisions and neutron stars. In addition to that, understanding the nature of the phase transition between a hadronic gas at low temperature and density and the quark gluon plasma at high  $T$  and  $\rho_B$  is an important problem in its own right and expected to shed some light on the vacuum structure of QCD.

While the structure of QCD at high temperature has been investigated in some detail using lattice simulations [1], little is known about matter at high baryon density. This is unfortunate, because the possible phase structure of matter at finite density is much richer, including phenomena such as pion [2] and kaon condensation [3], density isomers [4], strange quark matter [5], etc. From the point of view of lattice QCD, the difficulty is connected with the sign problem (see [6] for a recent review on lattice simulations at finite chemical potential). At zero temperature and chemical potential, the weight factor  $\det(\mathcal{D} + m) \exp(-S)$  in the euclidean path integral is real and positive. This means that the weight function can be interpreted as a probability distribution and one can perform simulations based on importance sampling. This remains true also at finite temperature. In euclidean space, the heat bath is represented by the (anti)periodic boundary conditions imposed on the gauge fields and fermions. At finite density, however, the determinant  $\det(\mathcal{D} + m - \mu\gamma_4)$  is complex and cannot be interpreted as a probability distribution.

Furthermore, while it is sometimes argued that neglecting the determinant (the so-called quenched approximation) provides a reasonable approximation at finite temperature, the same cannot be true at finite chemical potential. If the determinant is neglected, or if only the modulus of the determinant is retained, the critical chemical potential for chiral symmetry restoration is zero. This phenomenon is easily understood in the case where we retain the modulus only [7]. This approximation corresponds to a theory where half of the quarks couple with the opposite chemical potential. In this case, the lightest state that carries baryon number is a baryonic pion, a pion made of an ordinary quark and an

anti-quark that couples with the opposite chemical potential. This state is degenerate with the pion, so that in the chiral limit it can Bose condense even if the chemical potentials are arbitrarily small. In full QCD, on the other hand, the baryon density has to be zero as long as  $\mu < \mu_c \simeq M_B/3$ , where  $M_B$  is the mass of the lightest baryon.

Recently, this phenomenon has been studied in some detail in random matrix models of QCD [8–10]. While these models nicely illustrate the shortcomings of the quenched approximation they do not really improve our understanding of the phase transition in full QCD. The chemical potential is simply added as an external field to the random matrix that represents the Dirac operator. Chiral symmetry is restored when the chemical potential exceeds a certain critical value, but the dynamics of the phase transition is equivalent to a simple mean field model with static quarks [11].

In this work, we want to study QCD at finite chemical potential in the instanton liquid model. The instanton model is based on the assumption that the physics of chiral symmetry breaking and the dynamics of light hadrons is dominated by just a few low-lying modes in the spectrum of the Dirac operator. These modes are linear combinations of the zero modes associated with instantons, classical solutions of the euclidean Yang-Mills field equations. The instanton model provides a phenomenologically very successful description of the QCD vacuum, chiral symmetry breaking and hadronic correlation functions [12]. In addition to that, the underlying assumptions of the model can be checked in great detail on the lattice, see e.g. [13,14]. Of particular interest are recent simulations that focus on the correlation of low-lying eigenstates of the Dirac operator with topological charges, and on the role that these states play in the correlation functions of light hadrons [15–18]. There is evidence that low-lying states are approximately linear combinations of instanton zero modes, and that these states play a dominant role in the correlation functions of light mesons.

Studying instantons at finite chemical potential is worth while for several reasons. First, the model provides a very interesting mechanism for the chiral phase transition at finite temperature, based on the formation of topologically neutral instanton-anti-instanton pairs near  $T = T_c$  [19]. The corresponding eigenstates are localized modes, contrary to the

delocalized states that make up the quark condensate at  $T = 0$ . This scenario raises the question whether a similar mechanism might be at work at finite baryon density. Second, because the model concentrates on just a few modes in the spectrum of the Dirac operator, the sign problem should not be as severe as it is in lattice simulations. This should allow more realistic simulations to be performed. Finally, the instanton model can be studied in a number of approximations that allow for analytical (or almost analytical) solutions. In this case, one might be able to handle the analytic continuation required to introduce a chemical potential.

This paper is organized as follows. In Sect. 2 we discuss zero modes, the anomaly and the density of instantons at  $\mu \neq 0$ . In Sect. 3 we calculate matrix elements of the Dirac operator between zero mode wave functions. In Sect. 4, we study the spectrum of the Dirac operator in an ensemble of instantons at  $\mu \neq 0$ . In Sect. 5, we present simulations of the instanton liquid at small and large chemical potential.

## II. ZERO MODES AND THE ANOMALY AT $\mu \neq 0$

We would like to begin our discussion by constructing the free euclidean coordinate space propagators of bosons and fermions at non-zero chemical potential. This means that we are looking for solutions of the equations  $(i\partial_\alpha - i\delta_{\alpha 4}\mu)^2\Delta(x) = \delta(x)$  and  $(i\cancel{\partial} - i\mu\gamma_4)S(x) = \delta(x)$  subject to the appropriate boundary conditions. Naively, we can obtain solutions by multiplying the zero density propagator by  $\exp(\mu x_4)$ . This means that at finite chemical potential the propagation of quarks along the positive time direction (and anti-quarks along the negative time direction) is favored over propagation in the opposite direction.

However, this naive prescription does not provide the correct propagator. We have missed the contribution from occupied states below the Fermi surface. The correct solution is most easily obtained by Fourier transforming the momentum space propagator. The result for the charged Klein-Gordon propagator is

$$\Delta(x) = \frac{1}{4\pi^2} \frac{1}{r^2 + x_4^2} \left( \cos(\mu r) + \frac{x_4}{r} \sin(\mu r) \right). \quad (1)$$

Note that the extra contribution from occupied states has cancelled the exponent  $\exp(\mu x_4)$ .

From (1) we can also obtain the Fermion propagator

$$S(x) = (i\cancel{\partial} + i\mu\gamma_4) \Delta(x) = \frac{1}{4\pi^2 x^4} (\vec{\gamma} \cdot \hat{r} S_r(x) + \gamma_4 S_4(x)). \quad (2)$$

where the two functions  $S_r(x)$  and  $S_4(x)$  are given by

$$S_r(x) = (2r - \mu x^2 x_4/r) \cos(\mu r) + (x_4^4 + 3r^2 x_4 + \mu r^2 x^2) \frac{\sin(\mu r)}{r^2}, \quad (3)$$

$$S_4(x) = (2x_4 + \mu x^2) \cos(\mu r) + (x_4^2 - r^2 + \mu x_4 x^2) \frac{\sin(\mu r)}{r}. \quad (4)$$

Asymptotically, the propagator behaves as  $S(x_4) \sim \mu^2/x_4$  in the temporal direction, as compared to  $\sim 1/x_4^3$  at  $\mu = 0$ . The propagator in the positive  $x_4$  direction is still enhanced, but only by a power of  $x_4$  rather than an exponential. This enhancement is related to the fact that at finite  $\mu$ , quark paths dominantly wind around the imaginary time direction. The number of loops piercing an  $x_4 = \text{const}$  surface going forward in time, minus the number of loops going backwards, is related to the total baryon number. From (2) one easily reproduces the perturbative result  $\rho_B = 4S_4(r \rightarrow 0, x_4 = 0) = \mu^3/(3\pi^2)$ . In the next section we will also see that the anisotropy of the propagator causes the interaction between instantons to be strongly anisotropic as well.

For spacelike separations the propagator behaves as  $S(r) \sim \mu \sin(\mu r)/r^2$ . It decays as  $1/r^2$  and oscillates with a wave number given by the Fermi momentum  $p_F = \mu$ . The oscillations are due to the presence of a sharp Fermi surface and are analogous to Friedel oscillations in a degenerate electron gas [20,21].

Zero modes in the spectrum of the Dirac operator play a central role in understanding the  $U(1)_A$  anomaly and the mechanism for chiral symmetry breaking. While the relation to the anomaly is a rigorous consequence of the arguments given below, the connection with chiral symmetry breaking is more subtle. The Banks-Casher formula [22]  $\langle \bar{q}q \rangle = -\pi\rho(\lambda = 0)$  relates the density of eigenvalues of the Dirac operator at zero virtuality to the quark condensate. In a finite system with volume  $V$  these states are not exact zero modes, instead they occupy a band around zero with a typical level spacing  $\Delta\lambda \sim |\langle \bar{q}q \rangle|/V$  [23].

Perturbative states, on the other hand, are spaced much farther apart,  $\Delta\lambda \sim 1/V^{1/4}$ . It is tempting to identify the extra states with quasi zero modes that arise when the exact zero modes of isolated instantons and anti-instantons interact. The fact that this mechanism leads to chiral symmetry breaking was checked in simulations of the instanton ensemble in QCD [24,25]. Whether quasi zero modes associated with topology dominate the quark condensate in QCD is now under active investigation on the lattice [16,17,26], and initial results are very promising.

The connection of zero modes with the axial anomaly can be seen from the fact that the violation of axial charge in an arbitrary gauge potential is given by  $\Delta Q_5 = 2N_f(n_L - n_R)$ , where  $n_{L,R}$  is the number of left and right handed zero modes of the Dirac operator. Index theorems (or the anomaly equation  $\partial_\mu j_\mu^5 = N_f/(16\pi^2)G_{\mu\nu}\tilde{G}_{\mu\nu}$ ) then imply that zero modes have to be associated with topological charges. This requirement is satisfied by the instanton solution. The instanton has topological charge  $Q = +1$ , and the Dirac operator in the instanton field has a left-handed zero mode,  $i\mathcal{D}\psi_0 = 0$  and  $\gamma_5\psi_0 = -\psi_0$ . Analogously, there is a right handed zero mode in the field of an anti-instanton.

It is essential that these states are exact zero modes of the Dirac operator, because every non-zero mode automatically occurs in pairs and only unpaired states contribute to  $\Delta Q_5$ . If  $\psi_\lambda$  is an eigenstate of  $i\mathcal{D}$  with eigenvalue  $\lambda \neq 0$ , then  $\gamma_5\psi_\lambda$  is an eigenstate with eigenvalue  $-\lambda$ . This remains true at  $\mu \neq 0$ , because the extra term  $i\mu\gamma_4$  has the same chirality as  $i\mathcal{D}$ . But the anomaly is a short distance effect and should not be affected by a small chemical potential<sup>1</sup>. We therefore expect that there should be an exact zero mode in the spectrum of the Dirac operator in the instanton field also at  $\mu \neq 0$ .

This state can be found using the following observation [30]: Naively, a solution of the Dirac equation at  $\mu \neq 0$  is given by  $\exp(\mu x_4)\psi_0(x)$ , where  $\psi_0(x)$  is the  $\mu = 0$  zero mode. From our discussion of the quark propagator we expect that this is not an acceptable solution.

---

<sup>1</sup>See [27–29] for a similar discussion at finite temperature.

Instead, we have to construct a solution of the  $\mu = 0$  equation that cancels the exponential growth.

Such a solution can be found from the general ansatz [31]

$$\psi_0(x) = \frac{1}{2\sqrt{2}\pi\rho} \sqrt{\Pi(x)} \not{\partial} \left( \frac{\Phi(x)}{\Pi(x)} \right) U^{ab} \gamma_{\pm} \chi^b, \quad (5)$$

where  $\chi_i^a = \epsilon_{ia}$  is a Dirac and color spinor and  $\gamma_{\pm} = (1 \pm \gamma_5)/2$  for instantons/anti-instantons. The gauge potential of the instanton is given by  $A_{\nu} = \bar{\eta}_{\nu\rho}^a \partial_{\rho} \ln \Pi(x)$  where  $\bar{\eta}_{\mu\nu}^a$  is the anti-self-dual 't Hooft symbol [32] and  $\Pi(x) = 1 + \rho^2/x^2$ . For an anti-instanton, we have to make the usual replacement  $\bar{\eta}_{\mu\nu}^a \rightarrow \eta_{\mu\nu}^a$ . Substituting the ansatz (5) into the Dirac equation leads to the condition that  $\Phi(x)$  has to be a solution of the Laplace equation  $\square\Phi(x) = 0$ . At  $\mu = 0$ , a solution that is regular and satisfies the normalization condition is given by  $\Phi(x) = \rho^2/x^2$ .

This suggests that a solution which satisfies the boundary condition at finite chemical potential can be found from the  $\mu \neq 0$  Klein-Gordon propagator  $\Delta(x)$ . If  $\Delta(x)$  satisfies the Klein-Gordon equation with a chemical potential, then  $\Phi(x) = (4\pi^2)\rho^2 \exp(-\mu x_4)\Delta(x)$  is a solution of the Laplace equation that behaves as  $\Phi(x) \sim \exp(-\mu x_4)$ . It is easy to check that

$$\psi_0(x) = \sqrt{2}\pi\rho \exp(\mu x_4) \sqrt{\Pi(x)} \not{\partial} \left( \frac{\exp(-\mu x_4)\Delta(x)}{\Pi(x)} \right) U^{ab} \gamma_{\pm} \chi^b \quad (6)$$

indeed solves  $(i\not{D} - i\mu\gamma_4)\psi_0 = 0$  [30,33]. Furthermore, the zero mode solution is well behaved at infinity. It decays like the free quark propagator (2). Some care has to be taken in constructing the adjoint solution. The Dirac operator is not hermitean, so left eigenstates are not the hermitean conjugate of right eigenstates. In fact, it is easy to see that  $\psi_0^{\dagger}(\mu, x) = [\psi_0(-\mu, x)]^*$  is a solution of  $\psi_0^{\dagger}(i\not{D} - i\mu\gamma_4) = 0$ . Using this property, we can also check that the zero mode is correctly normalized,

$$\int d^4x \psi_0^{\dagger}(\mu, x)\psi_0(\mu, x) = 1. \quad (7)$$

In order to determine the importance of instanton effects at finite baryon density, we have to know the dependence of the instanton rate on the baryon chemical potential. At

large chemical potential, this dependence can be determined from a perturbative calculation. The result is<sup>2</sup> [30,35,36,34,33].

$$n(\rho, \mu) = n(\rho, 0) \exp\left(-N_f(\rho\mu)^2\right), \quad (8)$$

where  $n(\rho, 0)$  is the  $\mu, T = 0$  rate originally calculated by 't Hooft [32]. The suppression factor  $\exp(-N_f(\rho\mu)^2)$  is completely analogous to the factor  $\exp(-2(N_c/3 + N_f/6)(\pi\rho T)^2)$  that appears in the rate at finite  $T$  [37]. In both cases, the physical reason for the suppression of instantons is Debye screening of the strong  $O(1/g)$  color electric fields inside the instanton. The rate at  $T \neq 0$  contains some extra terms that are due to the fact that the instanton solution itself is deformed at  $T \neq 0$ . At least in perturbation theory, this effect is absent at  $\mu \neq 0$ .

Since the high temperature suppression factor is due to the scattering of perturbative quarks and gluons on the instanton, it was argued that the result should not be trusted at temperatures around and below  $T_c$  [38]. At low temperature the rate is determined by the scattering of hadrons, not quarks and gluons, on the instanton. This has been checked in lattice calculations of the temperature dependence of the topological susceptibility in quenched QCD [39–41]. These calculations find the expected exponential suppression above  $T_c$ , but below  $T_c$  the topological susceptibility is essentially independent of  $T$ .

Analogously, we expect that the result (8) is only valid if the chemical potential is large. At small baryon density, the rate is determined by the density dependence of the effective  $2N_f$ -fermion operator induced by instantons. In the case of small  $T$  and zero  $\mu$  this dependence can be determined from soft pion theorems [38]. At finite density, only the behavior of the quark condensate is known [42]

$$\langle \bar{q}q \rangle = \langle \bar{q}q \rangle \left\{ 1 - \frac{\Sigma_{\pi N}}{f_\pi^2 m_\pi^2} \rho_B + \dots \right\}, \quad (9)$$

where  $\Sigma_{\pi N} \simeq 46$  MeV is the  $\pi N$  sigma term. This implies  $\langle \bar{q}q \rangle \simeq \langle \bar{q}q \rangle_0 (1 - 0.3(\rho_B/\rho_B^0))$  where  $\rho_B^0 = 0.14 \text{ fm}^{-3}$  is nuclear matter density. If we estimate the density dependence

---

<sup>2</sup>See [34] for a discussion of the disagreements among some of the earlier calculations.

of the 't Hooft operator using factorization, we get a very rapid dependence,  $\langle \mathcal{O}_{tH} \rangle \simeq \langle \mathcal{O}_{tH} \rangle_0 (1 - 0.6(\rho_B/\rho_B^0))$  for  $N_f = 2$ . This seems too large, and factorization is not expected to be a good approximation at finite density. In order to improve on this estimate we have to determine the expectation value of the 't Hooft operator inside the nucleon. We have not performed this calculation, but it appears straightforward in principle. In practice, we have not used the perturbative result (8) in our simulations at small chemical potential, but we have taken it into account for large  $\mu$ .

### III. MATRIX ELEMENTS OF THE DIRAC OPERATOR

In order to study an ensemble of instantons at finite chemical potential, we have to determine matrix elements of the Dirac operator  $(i\mathcal{D} - i\mu\gamma_4)$  between the zero modes wave functions  $\psi_I$  associated with different instantons. At finite temperature, the functional form of these matrix elements plays a crucial role in determining the mechanism for the chiral phase transition. Near  $T_c$ , the overlap matrix elements favor the formation of polarized instanton-anti-instanton molecules [43,19]. Our aim here is to identify instanton configurations that may play a similar role at large chemical potential.

In the following, we will assume that the gauge potential of a system of instantons and anti-instantons can be approximated by the sum of the individual gauge potentials  $A_\nu = \sum_I A_\nu^I$ . In this case, the overlap matrix element is given by

$$T_{IA} = \int d^4x \psi_I^\dagger(x-z) (i\mathcal{D} - i\mu\gamma_4) \psi_A(x) = \int d^4x \psi_I^\dagger(x-z) (-i\cancel{\partial} + i\mu\gamma_4) \psi_A(x). \quad (10)$$

Here, we have used the equations of motion to reduce the covariant derivative to an ordinary one. Also note that because of the chirality of the zero modes, only matrix elements between instantons and anti-instantons are non-vanishing.

The overlap matrix elements  $T_{IA}$  depend on the distance  $z_\nu$  between the instantons, the instanton sizes  $\rho_{I,A}$  and the relative color orientation  $U = U_I^\dagger U_A$ . In the following, we will characterize the color orientation using the four-vector  $u_\nu = 1/(2i)\text{tr}(U\tau_\nu^{(+)})$ , where

$\tau_\nu^{(\pm)} = (\vec{\tau}, \mp)$ . At  $\mu, T = 0$ , Lorentz invariance implies that  $T_{IA} = i(u \cdot \hat{z})f(|z|, \rho_I, \rho_A)$ . At  $\mu, T \neq 0$ , Lorentz invariance is broken and the matrix elements have the more general structure (see [44,45] for a discussion of  $T_{IA}$  at  $T \neq 0$ )

$$T_{IA} = iu_4 f_1 + i(\vec{u} \cdot \hat{z}) f_2 \quad (11)$$

with  $f_i = f_i(|\vec{z}|, z_4, \rho_I, \rho_A)$  and  $\hat{z} = \vec{z}/|\vec{z}|$ . These functions can be calculated by writing the zero mode solutions in the form  $\psi_i^a = \phi_\nu(x)(\gamma_\nu)_{ij} U^{ab} \chi_j^b$ . At  $\mu, T = 0$ , we have  $\phi_\nu(x) = \hat{x}_\nu \phi(|x|)$ , while in the more general case  $\phi_\nu(x) = \delta_{\nu 4} \phi_4(r, x_4) + \delta_{\nu i} \hat{r}_i \phi_r(r, x_4)$ . In terms of  $\phi_\nu$ , the overlap matrix elements are given by

$$T_{IA} = 2iu_\alpha \int d^4x \left( \phi_\nu^A \partial_\nu \phi_\alpha^I - \phi_\nu^A \partial_\alpha \phi_\nu^I + \phi_\alpha^A \partial_\nu \phi_\nu^I - \mu \left( \phi_4^A \phi_\alpha^I - \delta_{\alpha 4} \phi_\nu^A \phi_\nu^I + \phi_\alpha^A \phi_4^I \right) \right), \quad (12)$$

where  $\phi_\nu^A = \phi_\nu(x - z)$  and  $\phi_\nu^I = \phi_\nu(x)$ . From (12) we can read off the invariant functions  $f_{1,2}$

$$f_1 = 2 \int d^4x \left\{ \phi_4^A \left( \partial_4 \phi_4^I + 2\phi_r^I/r + \partial_r \phi_r^I \right) + (\widehat{r-z}) \cdot \hat{r} \phi_r^A \left( \partial_r \phi_4^I - \partial_4 \phi_r^I \right) - \mu \left( \phi_4^A \phi_4^I - (\widehat{r-z}) \cdot \hat{r} \phi_r^A \phi_r^I \right) \right\}, \quad (13)$$

$$f_2 = 2 \int d^4x \left\{ \hat{z} \cdot (\widehat{r-z}) \phi_r^A \left( \partial_4 \phi_4^I + 2\phi_r^I/r + \partial_r \phi_r^I \right) + \hat{r} \cdot \hat{z} \phi_4^A \left( \partial_4 \phi_r^I - \partial_r \phi_4^I \right) - \mu \left( \hat{z} \cdot \hat{r} \phi_4^A \phi_r^I + \hat{z} \cdot (\widehat{r-z}) \phi_r^A \phi_4^I \right) \right\}. \quad (14)$$

The functions  $\phi_{r,4}$  are easily determined from (6) but the resulting integrals are fairly complicated and have to be performed numerically. Results are shown in Fig. 1 which also displays a simple parametrization of the matrix elements given in App. A. Similar results have been obtained by Rapp [46]. The most important point is that the asymptotics of  $T_{IA}$  are the same as those of the free quark propagator. In particular,  $T_{IA} \sim \mu^2/x_4$  in the time direction and  $T_{IA} \sim \mu \sin(\mu r)/r^2$  in the spatial direction.

In Sect. II we saw that at finite baryon density, quark paths tend to wind around the time direction. The probability of an instanton configuration is proportional to the fermion determinant, which contains the matrix elements  $T_{IA}$ . Since these matrix elements have the same functional form as the quark propagator, we also expect the instanton ensemble to be

dominated by instanton-anti-instanton chains that wind around the time direction. We will study this phenomenon in Sec. VI.

#### IV. THE INSTANTON ENSEMBLE AT $\mu \neq 0$

The instanton ensemble at finite baryon chemical potential is determined by the partition function

$$Z = \sum_{N_+, N_-} \frac{1}{N_+! N_-!} \int \prod_i^{N_+ + N_-} [d\Omega_i n(\rho_i)] \exp(-S_{int}) \prod_f^{N_f} \det(\mathcal{D} + m_f - \mu\gamma_4), \quad (15)$$

Here,  $N_+$  and  $N_-$  are the numbers of instantons and anti-instantons,  $\Omega_i$  the corresponding collective coordinates (position, color orientation and size), and  $n(\rho)$  the semi-classical size distribution. The bosonic interaction between instantons is denoted by  $S_{int}$  while the fermionic interaction is contained in the determinant  $\det(\mathcal{D} + m - \mu\gamma_4)$ .

Following the usual strategy in instanton model we will split the fermion determinant into a high and a low momentum part. The low momentum part is related to fermion zero modes and will be treated exactly. For the high momentum part we will assume that it can be factorized into the contributions of individual instantons. For a single instanton, the non-zero mode determinant in Gaussian approximation is included in the size distribution  $n(\rho)$ . The dynamics of the system is then governed by the determinant in the zero mode basis. At finite chemical potential, the Dirac operator has the structure

$$(i\mathcal{D} + i\mu\gamma_4)_{IJ} = \begin{pmatrix} 0 & T(\mu) \\ T^\dagger(-\mu) & 0 \end{pmatrix}, \quad (16)$$

where  $T$  is the matrix of overlap matrix elements  $T_{IA}$ . The block off-diagonal form of the Dirac operator is due to the chiral structure of the zero modes. Clearly, for  $\mu \neq 0$  the Dirac operator is not hermitean and its eigenvalues are complex.

For comparison, the form of the Dirac operator in a basis of  $\mu = 0$  zero modes is

$$(i\mathcal{D} + i\mu\gamma_4)_{IJ} = \begin{pmatrix} 0 & T(\mu=0) + \mu M(\mu=0) \\ T^\dagger(\mu=0) - \mu M^\dagger(\mu=0) & 0 \end{pmatrix}, \quad (17)$$

where  $M_{IA}$  are matrix elements of  $\gamma_4$ . This is the structure of the Dirac operator that is assumed in random matrix models of QCD at finite chemical potential (with the additional simplification  $M \rightarrow 1$ ) [8].

We will study the difference between the exact matrix elements (16) and the simplified version (17) in Sec. VI. But even without a calculation it is clear that the full matrix elements can carry significant dynamics whereas in the simplified form (in particular if the substitution  $M \rightarrow 1$  is made) the chemical potential only acts like an external field. The situation is similar to what happens at finite temperature. While random matrix models provide a good description of the dynamics of zero modes at  $T = 0$  (and  $N_f$  not too large), the dynamics of the phase transition is very different (see [47] for a random matrix model that mimics the phase transition in the instanton model). There is one more important difference between the Dirac operators (16) and (17): For  $\mu \rightarrow \infty$  the schematic Dirac operator (17) becomes anti-hermitean, so all eigenvalues are imaginary and the determinant is real. For the exact zero modes, on the other hand, the Dirac operator does not simplify in that limit.

The statistical system described by the partition function (15) is quite complicated so that in general one has to rely on numerical simulations to determine the phase structure. At finite temperature and zero chemical these simulations are straightforward [48], but at finite chemical potential one has to deal with the fact that the determinant is complex.

At this point, the only practical solution to this problem is to generate an ensemble with the absolute magnitude of the determinant

$$Z_{||} = \sum_{N_+, N_-} \frac{1}{N_+! N_-!} \int \prod_i^{N_+ + N_-} [d\Omega_i n(\rho_i)] \exp(-S_{int}) \left| \prod_f^{N_f} \det(\mathcal{D} + m_f - \mu\gamma_4) \right|, \quad (18)$$

and incorporate the phase information into the observables. This means that expectation values are determined from

$$\langle \mathcal{O} \rangle = \frac{\langle e^{i\phi} \mathcal{O} \rangle_{||}}{\langle e^{i\phi} \rangle_{||}}, \quad (19)$$

where  $\langle \cdot \rangle_{||}$  is an expectation value determined with the modulus of the determinant and  $\phi$  is the phase of the determinant. As mentioned in the introduction, taking into account the

phase information is absolutely essential. The theory described by the partition function with the modulus of the determinant is very different from QCD. In particular, we expect chiral symmetry restoration to take place at  $\mu \simeq m_\pi/2$ .

The problem with this method is that if fluctuations in the phase are large then  $\langle e^{i\phi} \rangle$  will typically be close to zero and the expectation value (19) is essentially undetermined. In other words, if fluctuations are big then the ensemble generated by (18) has a very small overlap with the correct ground state.

An important simplification occurs in the special case of two colors,  $N_c = 2$ . In this case, the matrix elements  $T_{IA}$  are real (because the color orientation vector  $u_\mu$  is real). Eigenvalues not only occur in pairs  $\pm\lambda$ , but also in complex conjugate pairs  $\lambda, \lambda^*$ . Not all eigenvalues are four-fold degenerate because some of them are purely real or purely imaginary. This means that the determinant is real, but not necessarily real and positive. We can construct a theory with a real and positive determinant by considering the case  $N_c = 2$  and  $N_f$  even.

Since the determinant is positive, QCD with  $N_c = 2$  and  $N_f = 2$  is easy to simulate even if the chemical potential is non-zero. But as in the case of quenched QCD, the physics is very different from real QCD. If  $N_c = 2$ , baryons are diquarks. Furthermore, the  $N_c = 2$  theory has an additional particle-anti-particle (Pauli-Gürsey) symmetry [49,50] symmetry which implies that the scalar diquark is degenerate with the pion. This means that the critical chemical potential is again expected to be  $\mu \simeq m_\pi/2$ .

## V. SPECTRUM OF THE DIRAC OPERATOR AT FINITE CHEMICAL POTENTIAL

The low virtuality part of the Dirac spectrum is intimately connected with the physics of chiral symmetry breaking. For  $\mu = 0$ , this is expressed by the Banks-Casher relation

$$\langle \bar{q}q \rangle = -\pi\rho(\lambda=0), \tag{20}$$

which relates the quark condensate in the chiral limit to the spectral density of the Dirac operator,  $\rho(\lambda) = \langle \sum_i \delta(\lambda - \lambda_i) \rangle$ . For non-zero chemical potential, the eigenvalues are complex

and  $\rho(\lambda)$  is a density in the complex plane. How to interpret the Banks-Casher relation in that case was explained by Stephanov [8]: The quark condensate is related to the resolvent of the Dirac operator,  $\langle \bar{q}q \rangle = G(i0)$  where  $G(z) = \langle \text{tr}(i\mathcal{D} + z)^{-1} \rangle$  defines a function in the complex plane. The vector field  $\vec{G} = (\text{Re}G, -\text{Im}G)$ , can be interpreted as the “electric field” generated by the “charge density”  $\rho(z)$ . If quarks are condensed this function has a discontinuity on the real line. This means that there has to be a finite density of eigenvalues on that line.

If the chemical potential is smaller than the critical value where the baryon density becomes non-zero the quark condensate has to be independent of  $\mu$ . This means that while in general eigenvalues will spread in the complex plane, eigenvalues near zero virtuality have to stay on the real line. As soon as  $\mu > \mu_c$ , some of the small eigenvalues can move into the complex plane, but the density of eigenvalues on the real line has to remain finite. Only above the critical chemical potential for chiral symmetry restoration can all eigenvalues spread out in the complex plane.

In the remainder of this section we will discuss eigenvalue distributions in the instanton liquid model. These distributions were obtained from numerical simulations of the partition function (18). For simplicity, we have kept the instanton density  $(N/V) = 1 \text{ fm}^{-4}$  fixed. In principle, the correct equilibrium density is determined by minimizing the free energy. This can be done using the methods discussed in [48], but is beyond the scope of our exploratory study.

Fig. 2 shows scatterplots of eigenvalues of the Dirac operator obtained in quenched simulations for  $N_c = 2, 3$  and  $\mu = 1 \text{ fm}^{-1}$ . For  $N_c = 3$ , the eigenvalues spread almost uniformly over a band in the complex plane. In the case of two colors, there is a finite fraction of eigenvalues that stays on the real line. This phenomenon was also observed in random matrix models [51]. From our discussion above that would seem to indicate that for  $N_c = 2$  chiral symmetry remains broken, while for  $N_c = 3$  chiral symmetry is restored. This is not the case. Chiral symmetry restoration in the case of three colors is an artefact of the quenched approximation. For  $N_c = 2$  the density of eigenvalues on the real line vanishes in

the infinite volume limit. We will study this case in more detail in the next section.

For  $N_c = 2$  the unquenched eigenvalue distribution is qualitatively similar to the quenched distribution. This is not true for  $N_c = 3$ . In order to calculate the unquenched eigenvalue distribution we have binned the eigenvalues and determined the average number of eigenvalues per bin from numerical simulations of the partition function (18). The unquenched distribution is then obtained by including the phase of the determinant according to (19). In general, this procedure will give a complex eigenvalue density but in our simulations the imaginary part was always consistent with zero.

In Fig. 3 we show the density of eigenvalues for  $\mu = 1.0 \text{ fm}^{-1}$  without the phase (upper panel) and with the phase included (lower panel). We observe that if the phase is included, the number of eigenvalues away from the real line near  $\lambda = 0$  is reduced. This is clearly the correct tendency although with our statistics, we cannot really determine whether there is a discontinuity on the real line. We will study the quark condensate more quantitatively in the next section.

## VI. CHIRAL SYMMETRY RESTORATION IN THE INSTANTON LIQUID

In this section we wish to study the quark condensate in unquenched simulations of the instanton liquid at finite chemical potential. Let us start with the simpler case  $N_c = 2$ ,  $N_f = 2$ . In Fig. 4 we show the quark condensate and the fraction of real eigenvalues as a function of the chemical potential for different volumes  $V = 16, 32, 64 \text{ fm}^4$ . The instanton density was fixed at  $(N/V) = 1 \text{ fm}^{-4}$  and the quark mass is  $m = 20 \text{ MeV}$ . This mass is somewhat larger than the physical quark mass and was chosen to minimize finite volume effects. We observe that the quark condensate decreases as  $\mu$  increases and that chiral symmetry is restored for large chemical potentials. While the number of real eigenvalues decreases as the volume is increased, the behavior of the quark condensate does not change appreciably. This would seem to indicate that for finite quark masses, there is no sharp transition in the infinite volume limit.

The behavior of the quark condensate and the chiral susceptibility  $\chi_\sigma = V(\langle(\bar{q}q)^2\rangle - \langle\bar{q}q\rangle^2)$  for different quark masses  $m = 20, 30, 40$  MeV is shown in Fig. 5. We have also determined the  $\mu = 0$  pion mass for these quark masses. We find  $m_\pi \simeq 240, 280, 360$  MeV, with statistical errors  $\Delta m_\pi \simeq 20$  MeV. The onset  $\mu_0$  of chiral symmetry restoration is hard to determine from the data, but the results appear to be consistent with  $\mu_0 \simeq m_\pi/2$ . We also observe that the pseudo-critical chemical potential  $\mu_c$  (determined from the peak of the chiral susceptibility) drops with the quark mass. Again the errors are large, but the behavior is compatible with  $\mu_c \sim \sqrt{m}$ .

For large chemical potential the quark condensate goes to zero but we expect that diquarks are condensed. This idea is based on the fact that  $SU(2)$  gauge theory with two massless flavors has an extra symmetry that relates the chiral condensate  $\langle\bar{q}^a q^a\rangle$  to the scalar diquark condensate  $\langle\epsilon^{ab} q^a C \gamma_5 \tau_2 q^b\rangle$ . Here,  $C$  is the charge conjugation matrix,  $a, b$  are color labels and  $\tau_2$  is the anti-symmetric Pauli matrix (the diquark is an iso-singlet). A finite quark mass breaks the symmetry and favors quark-anti-quark over diquark condensation. For large chemical potential, on the other hand, we expect that diquark condensation is favored. This scenario was first discussed in the context of the strong coupling limit by Dagotto et al. [52]. However, these authors concluded that chiral symmetry remains broken for large  $\mu$ . In general, this is not correct. For  $N_f = 2$  the diquark condensate is a chiral singlet. For more than two flavors, on the other hand, part of the chiral symmetry is broken<sup>3</sup>.

Let us now study the more interesting case  $N_c = 3$ . We have performed simulations with the Dirac operator evaluated in a basis of exact  $\mu \neq 0$  zero modes (16) and with the schematic Dirac operator (17). The results presented here were obtained by generating 5000 configurations in a volume  $V = 16 \text{ fm}^4$ . In addition to that, some runs were performed with  $V = 32 \text{ fm}^4$ . To illustrate the procedure, we show trajectories of the quark condensate and the phase of the determinant for 400 Monte Carlo sweeps at  $\mu = 0.5 \text{ fm}^{-1}$  in Fig. 6. The

---

<sup>3</sup>Dagotto et al. use staggered fermions, so effectively the number of flavors is a multiple of 4

fluctuations are larger as compared to the  $\mu = 0$  case, but  $\langle e^{i\phi} \rangle$  is still differs significantly from zero. If  $\mu > 1 \text{ fm}^{-1}$  the fluctuations are so large that both the real and imaginary parts of  $\langle e^{i\phi} \rangle$  are close to zero.

Fig. 7 shows the real parts of the quark condensate and the average phase  $\langle e^{i\phi} \rangle$  calculated with the  $\mu = 0$  zero modes. The imaginary part of both quantities is always consistent with zero. We display both  $\langle \bar{q}q \rangle$  and  $\langle \bar{q}q \rangle_{||}$ , the quark condensate with and without fluctuations of the phase of the determinant taken into account.

We observe that  $\langle \bar{q}q \rangle_{||}$  drops rapidly with  $\mu$ . This is the expected artefact that comes from neglecting the phase of the determinant. With the phase taken into account,  $\langle \bar{q}q \rangle$  becomes almost independent of the chemical potential for  $\mu < 1 \text{ fm}^{-1}$ . In general we expect  $\langle \bar{q}q \rangle$  to be  $\mu$ -independent for  $\mu < \mu_c$  with  $\mu_c \simeq m_B/3 \simeq 1.5 \text{ fm}^{-1}$ . In the instanton model this is not quite true, because the most tightly bound state that carries baryon number is a scalar diquark, so  $\mu_c \simeq m_D/2$ .

The data show a small but statistically significant rise in  $\langle \bar{q}q \rangle$  for  $\mu < 1 \text{ fm}^{-1}$ . The result is not a finite volume effect because it is also present in the  $V = 32 \text{ fm}^4$  data. A similar phenomenon was also observed in random matrix models [10], where it was argued that the problem is related to the restriction to a finite number of static modes.

For chemical potentials larger than  $\mu \simeq 1 \text{ fm}^{-1}$  the complex phase becomes very small and  $\langle \bar{q}q \rangle$  has very large error bars. Without the phase, the quark condensate is small and fluctuates little. This is due to the fact that the eigenvalues of the Dirac operator are pushed farther and farther away from the real line, see Fig. 2b. If the chemical potential is very large,  $\mu > 5 \text{ fm}^{-1}$ , the complex phase factor starts to grow and  $\langle \bar{q}q \rangle$  can again be determined. The reason for this behavior is trivial and was already discussed in Sect. IV: If  $\mu M_{IA}$  is much bigger than the typical overlap matrix element  $T_{IA}$ , the Dirac operator becomes anti-hermitean and all eigenvalues are close to the imaginary line<sup>4</sup>.

---

<sup>4</sup>Note that we have performed these simulations without the exponential suppression factor (8).

In Fig. 8 we show the results for the Dirac operator evaluated in the basis of exact  $\mu \neq 0$  zero modes. Again,  $\langle \bar{q}q \rangle_{||}$  drops rapidly with  $\mu$ . Including the phase helps to stabilize the quark condensate, but there is a definite drop in  $\langle \bar{q}q \rangle$  even for  $\mu < 1 \text{ fm}^{-1}$ . In this case, the effect becomes smaller as we go to larger volumes. We therefore believe that the effect is mostly due to the onset of chiral symmetry restoration near  $\mu_c \simeq 1 \text{ fm}^{-1}$ , smeared out by finite volume effects.

For  $\mu > 1 \text{ fm}^{-1}$  the complex phase factor again becomes very small and we cannot perform reliable simulations. However, for  $\mu > 3 \text{ fm}^{-1}$  the phase factor  $\langle e^{i\phi} \rangle$  starts to grow and simulations are feasible. In the plasma phase, chemical potentials between  $(2 - 3) \text{ fm}^{-1}$  correspond to a baryon density  $n_B = 2\mu^3/(3\pi^2) = (0.5 - 1.8) \text{ fm}^{-3}$ . In this regime the quark condensate is very small and the instanton ensemble is in the chirally restored phase. It is interesting to analyze the mechanism that causes the symmetry to be restored.

For this purpose we show two typical instanton configurations for  $\mu = 0$  and  $\mu = 5 \text{ fm}^{-1}$  in Fig. 9. The figures show projections of a four dimensional box into the  $x_3 - x_4$  plane. The locations of instantons and anti-instantons are denoted by  $\pm$  signs, and the strength of the fermionic overlap matrix elements  $T_{IA}$  are indicated by the thickness of the lines connecting the instantons. We observe that for  $\mu = 0$  instantons are distributed randomly and there is no particular pattern to the lines connecting them. This is a sign for chiral symmetry breaking. If instantons tend to form large random clusters, then the corresponding eigenfunctions will be low-lying delocalized modes. These are the modes that form the quark condensate.

At large chemical potential, instantons tend to line up in the  $x_4$ -direction. These chains are weakly linked in the spatial direction. The reason why these configurations are favored

---

This was done for consistency, because (17) is really a small  $\mu$  approximation. Including the suppression factor also has the unusual effect that  $\mu M_{IA}$  never dominates over  $T_{IA}$ , because  $T_{IA} \sim \rho^{-1}$  and the factor  $\exp(-N_f(\mu\rho)^2)$  in the instanton rate forces  $\rho^{-1} > \mu$ .

should be clear from our discussion of the overlap matrix elements in Sect. III: For large  $\mu$ ,  $T_{IA}$  is big in the temporal direction and oscillates for spacelike separations. There are two reasons why these configurations tend to have an almost real determinant. One is the fact that for the most attractive orientation, we have  $u_4 = 1$  and the overlap matrix element is real. The other is that the dominant terms in  $T_{IA}$  at large chemical potential are even in  $\mu$ , corresponding to an almost hermitean Dirac operator.

For the chain-like configurations observed at large chemical potential, chiral symmetry is restored because the eigenfunctions tend to be spatially localized. This can be seen from Fig. 10 which shows the distribution of participation numbers of the low-lying eigenstates for three different simulations at  $T = \mu = 0$ ,  $T \simeq T_c$  and  $\mu = 0$  [48], and  $T = 0$ ,  $\mu > \mu_c$ . The participation number is a concept borrowed from the theory of localization (Mott-Anderson) phase transitions [53]. For a normalized eigenvector  $c_i$ , we define the participation number

$$P = 1 / \sum_i |c_i|^4 \quad \left( \sum_i |c_i|^2 = 1 \right). \quad (21)$$

The participation number is a measure of the number of (localized) basis states that contribute to an eigenstate of the system. We observe that at  $\mu = T = 0$  many basis states participate in the low-lying eigenstates. In fact, the participation number of these states grows with the volume of the system. The finite  $T$  transition is associated with the formation of instanton-anti-instanton molecules and the dominant participation number near  $T_c$  is two. In the finite  $\mu$  transition we also observe that the average participation number becomes smaller, but the average cluster size is bigger than two. One can check that the size of these clusters is dominantly controlled by the inverse temperature (the length of the imaginary time direction). We conclude that the system is dominated by oriented instanton “polymers”.

In more physical terms, chiral symmetry restoration is due the presence of valence quarks in the system. Valence quarks can saturate the fermionic bonds between instantons. If the density of valence quarks is sufficiently large all bonds are saturated, and additional quarks can no longer propagate from one instanton to another. As a result, quarks do not acquire a

constituent mass and chiral symmetry is restored. This interpretation becomes more obvious if one reduces the instanton-induced interaction between quarks to an effective four-fermion interaction, and treats this interaction in the mean-field approximation (see, e.g. [54]). Chiral symmetry breaking is then described in terms of a gap equation for the constituent quark mass. At large density chiral symmetry is restored because valence quarks Pauli-block the quark loop that drives the formation of a constituent mass.

## VII. SUMMARY

In summary we have studied instantons and their interactions at finite baryon chemical potential. We have emphasized the importance of exact zero modes in the spectrum of the Dirac operator even at  $\mu \neq 0$ . We have determined matrix elements of the Dirac operator between zero modes associated with different instantons. These matrix elements favor the propagation of quarks along the positive  $x_4$  direction.

Using these ingredients we have performed a number of exploratory simulations of the instanton liquid at finite chemical potential. In the case  $N_c = 2$  and  $N_f = 2$  these simulations are straightforward because the theory does not have sign problem. We observe that chiral symmetry is restored at  $\mu_c \sim \sqrt{m}$ . The high density state is likely to support a diquark condensate.

For  $N_c = 3$  the simulations are complicated by the sign problem. In our simulations we focus on the dynamics of (quasi) zero modes. This means that number of degrees of freedom in a given volume is much smaller than in a typical lattice simulation and the sign problem is not as severe. In practice we can perform simulations in sufficiently large volumes for  $\mu < 1 \text{ fm}^{-1}$  and  $\mu > 3 \text{ fm}^{-1}$ . For small chemical potential we observe that including the phase of the determinant has the correct effect of stabilizing the quark condensate. Qualitatively, this is true for both the ensemble generated with the  $\mu = 0$  and the correct  $\mu \neq 0$  zero modes. Quantitatively, the quark condensate rises for small  $\mu$  in the first case, while there is a tendency towards chiral restoration in the other case.

The structure of the chirally restored phase at large  $\mu$  is completely determined by the functional form of the zero mode wave functions. In schematic models of the structure of the Dirac operator, the fluctuations in the phase become small because for large  $\mu$  the determinant is dominated by the chemical potential term. Chiral symmetry is restored because the large external field pushes all eigenvalues away from zero. In the instanton liquid, fluctuations become small because the ensemble is dominated by chain-like configurations for which the determinant is almost real. Chiral symmetry is restored because the corresponding eigenfunctions are strongly localized.

Much more work remains to be done in order to understand the nature of the chirally restored phase at large chemical potential and the onset of chiral restoration at small  $\mu$ . In particular, we have to study the quark propagator, mesonic correlation functions and the thermodynamics of the system at large  $\mu$ . This should clarify whether there is any tendency towards diquark condensation, strange matter formation, etc.

We should also point out the shortcomings of our procedure. The restriction of the determinant to quasi zero modes has enabled us to perform simulations in reasonably large volumes but it also introduces certain artefacts. For example, non-zero modes have to contribute to the total baryon number of the system. Also, if non-zero modes are neglected the quark condensate is not necessarily independent of  $\mu$  below  $\mu_c \simeq m_B/3$ . Finally, as long as there is no real solution to the sign problem, simulations in the interesting regime  $\rho_B \simeq \rho_B^0$  will remain impossible.

Acknowledgements: I would like to thank R. Rapp, E. Shuryak, M. Velkovsky and J. Verbaarschot for useful discussions.

## APPENDIX A: FERMIONIC OVERLAP MATRIX ELEMENTS

The two functions  $f_{1,2}$  depend on the instanton-anti-instanton distance  $(\vec{z}, z_4)$ , the two radii  $\rho_{I,A}$  and the chemical potential  $\mu$ . If the two radii are equal, it is clear that  $f_i$  only depends on  $|\vec{z}|/\rho$ ,  $z_4/\rho$  and  $\mu\rho$ . We have checked numerically that if  $\rho_I \neq \rho_A$  the matrix elements depend to a very good accuracy only on the geometric mean  $\bar{\rho} = \sqrt{\rho_I\rho_A}$ .

This leaves us with two functions  $f_i(\tilde{z}_r, \tilde{z}_4, \tilde{\mu})$ , where  $\tilde{z}_r = z_r/\bar{\rho}$ , etc. are dimensionless variables. We have determined these functions numerically for many different values of the variables and fitted the result to the following parametrizations

$$f_1 = \frac{2.0}{(2.2 + z^2)^2} \left\{ (2z_4 + a_1\mu z_4^2 + a_2\mu z_r^2 + a_3\mu^2 z_4) \cos(\mu z_r) \right. \\ \left. - (a_4\mu^2 + a_5 z_r^2 - a_6 z_4^2 - a_7\mu z_4 z_2) \frac{\sin(\mu z_r)}{z_r} + a_8\mu^2 \sin(\mu z_r) \right\}, \quad (\text{A1})$$

$$f_2 = \frac{2.0}{(2.2 + z^2)^2} \left\{ (2z_r - b_1\mu z_4^3/z_r + b_2\mu z_4 z_r + b_3\mu^2 z_r^2) \cos(\mu z_r) \right. \\ \left. + (b_1 z_4^3 + 3b_4 z_r^2 z_4 + b_5\mu z_r^4 + b_6\mu z_r^2 z_4^2) \frac{\sin(\mu z_r)}{z_r^2} + (b_7\mu + b_8\mu^2 z_4) \sin(\mu z_r) \right\}, \quad (\text{A2})$$

where we have dropped the tilde symbol. The functional form of the parametrizations was inspired by the free quark propagator (2). In addition to that we have to respect the symmetries  $f_i(z, \mu) = \mp f_i(-z, -\mu)$ , ( $i=1,2$ ) of the matrix elements and ensure the correct behavior for  $\mu \rightarrow 0$ .

Fitting the parametrization (A1,A2) to the data, we get

$$a_1 = 1.334, \quad a_2 = 2.142, \quad a_3 = 2.872, \\ a_4 = 0.756, \quad a_5 = 2.378, \quad a_6 = 0.893, \\ a_7 = 1.060, \quad a_8 = -0.845, \quad (\text{A3})$$

$$b_1 = 2.361, \quad b_2 = 1.561, \quad b_3 = 0.072, \\ b_4 = 1.027, \quad b_5 = 0.818, \quad b_6 = 0.844, \\ b_7 = 3.270, \quad b_8 = 1.313. \quad (\text{A4})$$

The quality of the fit can be judged from the results shown in Fig. 1 and appears quite satisfactory for our purposes.

## REFERENCES

- [1] C. DeTar, 1995. in *Quark Gluon Plasma 2*, edited by R. Hwa, World Scientific, Singapore.
- [2] A. B. Migdal. *Soviet Phys., JETP*, 34:1184, 1972.
- [3] D. B. Kaplan and A. E. Nelson. *Phys. Lett.*, B175:57, 1986.
- [4] T. D. Lee. *Rev. Mod. Phys.*, 47:267, 1975.
- [5] E. Witten. *Phys. Rev.*, D30:272, 1984.
- [6] I. M. Barbour, S. E. Morrison, E. G. Klepfish, J. B. Kogut, and M.-P. Lombardo. 1997. hep-lat/9705042.
- [7] A. Gocksch. *Phys. Rev.*, D37:1014, 1988.
- [8] M. A. Stephanov. *Phys. Rev. Lett.*, 76:4472, 1996.
- [9] R. A. Janik, M. A. Nowak, G. Papp, and I. Zahed. *Phys. Rev. Lett.*, 77:4876, 1996.
- [10] M. A. Halasz, A. D. Jackson, and J. J. M. Verbaarschot. 1997. hep-lat/9703006.
- [11] R. Janik, M. A. Nowak, and I. Zahed. *Phys. Lett.*, B392:155, 1997.
- [12] T. Schäfer and E. V. Shuryak. *Rev. Mod. Phys.*, *in press*, 1997. hep-ph/9610451.
- [13] M. C. Chu, J. M. Grandy, S. Huang, and J. W. Negele. *Phys. Rev.*, D49:6039, 1994.
- [14] C. Michael and P. S. Spencer. *Phys. Rev.*, D52:4691, 1995.
- [15] S. Thurner, M. Feurstein, H. Markum, and W. Sakuler. *Phys. Rev.*, D54:3457, 1996.
- [16] T. L. Ivanenko and J. W. Negele. 1997. hep-lat/9709130.
- [17] T. DeGrand, A. Hasenfratz, and T. G. Kovacs. 1997. hep-lat/9710078.
- [18] L. Venkataraman and G. Kilcup. 1997. hep-lat/9710086.

- [19] T. Schäfer, E. V. Shuryak, and J. J. M. Verbaarschot. *Phys. Rev.*, D51:1267, 1995.
- [20] J. Kapusta and T. Toimela. *Phys. Rev.*, D37:3731, 1988.
- [21] W. Florkowski and B. Friman. *Nucl. Phys.*, A611:409, 199.
- [22] T. Banks and A. Casher. *Nucl. Phys.*, B169:103, 1980.
- [23] H. Leutwyler and A. Smilga. *Phys. Rev.*, D46:5607, 1992.
- [24] E. V. Shuryak and J. J. M. Verbaarschot. *Nucl. Phys.*, B341:1, 1990.
- [25] J. J. M. Verbaarschot. *Nucl. Phys.*, B427:534, 1994.
- [26] S. Thurner, M. Feurstein, and H. Markum. 1996. preprint, hep-lat/9606011.
- [27] T. Schäfer. *Phys. Lett.*, B389:445, 1996.
- [28] S. H. Lee and T. Hatsuda. *Phys. Rev.*, D54:1871, 1996.
- [29] N. Evans, S. D. H. Hsu, and M. Schwetz. *Phys. Lett.*, B375:262, 1996.
- [30] C. A. De Carvalho. *Nucl. Phys.*, B183:182, 1980.
- [31] B. Grossman. *Phys. Lett.*, A61:86, 1977.
- [32] G. 't Hooft. *Phys. Rev.*, D14:3432, 1976.
- [33] A. A. Abrikosov. *Sov. J. Nucl. Phys.*, 37:459, 1983.
- [34] E. V. Shuryak. *Nucl. Phys.*, B203:140, 1982.
- [35] V. Baluni. *Phys. Lett.*, 106B:491, 1981.
- [36] M. Chemtob. *Nucl. Phys.*, B184:497, 1981.
- [37] D. J. Gross, R. D. Pisarski, and L. G. Yaffe. *Rev. Mod. Phys.*, 53:43, 1981.
- [38] E. V. Shuryak and M. Velkovsky. *Phys. Rev.*, D50:3323, 1994.
- [39] M. C. Chu and S. Schramm. *Phys. Rev.*, D51:4580, 1995.

- [40] E.-M. Ilgenfritz, M. Müller-Preußker, and E. Meggiolaro. *Nucl. Phys. (Proc. Suppl.)*, B42:496, 1995.
- [41] B. Alles, M. D’Elia, and A. DiGiacomo, 1997.
- [42] E. G. Drukarev and E. M. Levin. *Sov. Phys. JETP*, 68:680, 1989.
- [43] E.-M. Ilgenfritz and E. V. Shuryak. *Phys. Lett.*, B325:263, 1994.
- [44] E. V. Shuryak and J. J. M. Verbaarschot. *Nucl. Phys.*, B364:255, 1991.
- [45] V. Khoze and A. Yung. *Z. Phys.*, C50:155, 1991.
- [46] R. Rapp. 1997. private communication.
- [47] T. Wettig, A. Schäfer, and H. Weidenmüller. *Phys. Lett.*, B367:28, 1996.
- [48] T. Schäfer and E. V. Shuryak. *Phys. Rev.*, D53:6522, 1996.
- [49] W. Pauli. *Nuovo Cim.*, 6:205, 1957.
- [50] F. Gürsey. *Nuovo Cim.*, 7:411, 1958.
- [51] M. A. Halasz, J. C. Osborn, and J. J. M. Verbaarschot. 1997. hep-lat/9704007.
- [52] E. Dagotto, F. Karsch, and A. Moreo. *Phys. Lett.*, 169B:421, 1986.
- [53] B. Kramer and A. MacKinnon. *Rep. Prog. Phys.*, 56:1469, 1993.
- [54] S. Klimt, M. Lutz, and W. Weise. *Phys. Lett.*, B249:386, 1990.

## FIGURES

FIG. 1. Overlap matrix elements  $f_{1,2}$  as a function of the instanton-antiinstanton separation  $z$  in units of  $\rho$ . Fig. a) shows  $f_1$  as a function of  $z_4$  for  $z_r = 0$ , while Fig. b) shows  $f_2$  as a function of  $z_r$  for  $z_4 = 0$ . The points are numerical results for the overlap integrals while the lines show the parametrization discussed in the appendix. The solid, long-dashed, and short-dashed curves correspond to  $(\mu\rho) = 0, 1, 2$ .

FIG. 2. Scatterplots of the complex eigenvalues of the Dirac operator from quenched simulations at  $\mu = 1 \text{ fm}^{-1}$  for  $N_c = 2$  and  $N_c = 3$ .

FIG. 3. Contourplots of the eigenvalue density in the complex plane from unquenched simulations at  $\mu = 1 \text{ fm}^{-1}$  without (upper panel) and with (lower panel) the phase of the determinant included. The  $x$  and  $y$  axes show the real and imaginary parts of the eigenvalues.

FIG. 4. Quark condensate (upper panel) and fraction of real eigenvalues (lower panel) as a function of the chemical potential for  $N_c = 2$ ,  $N_f = 2$  from numerical simulation of the unquenched theory. The different curves correspond to different volumes  $V = 16, 32, 64 \text{ fm}^4$ .

FIG. 5. Quark condensate (upper panel) and scalar susceptibility (lower panel) as a function of the chemical potential in  $N_c = 2$ ,  $N_f = 2$  QCD. The different curves show the results for different quark masses  $m = 10, 20 \text{ MeV}$  with the volume  $V = 32 \text{ fm}^4$  kept fixed.

FIG. 6. Time history of the quark condensate (both real and imaginary parts) and the cosine of the phase of the fermion determinant for an instanton liquid simulation at  $\mu = 0.5 \text{ fm}^{-1}$ . The figure shows 400 configurations generated in a volume  $V = 16 \text{ fm}^4$ .

FIG. 7. Quark condensate (upper panels) and average phase of the fermion determinant (lower panels) as a function of the chemical potential for  $N_c = 3$ ,  $N_f = 2$  from numerical simulation of the unquenched theory. The open and solid points show the quark condensate without and with the phase included. The calculations shown here were performed in the  $\mu = 0$  basis equ. (17).

FIG. 8. Same as Fig. (7) with the determinant evaluated in the  $\mu \neq 0$  basis (16).

FIG. 9. Typical instanton configurations for  $\mu = 0$  and  $\mu = 5 \text{ fm}^{-1}$ . The plots show projections of a four dimensional box into the  $x_3 - x_4$  plane. The positions of instantons and anti-instantons are shown as  $\pm$  symbols. The lines indicate the strength of the fermionic overlap matrix elements  $T_{IA}$ .

FIG. 10. Distribution of participation numbers for low-lying eigenvectors in the instanton liquid at finite temperature (upper panel), and at finite chemical potential (lower panel).

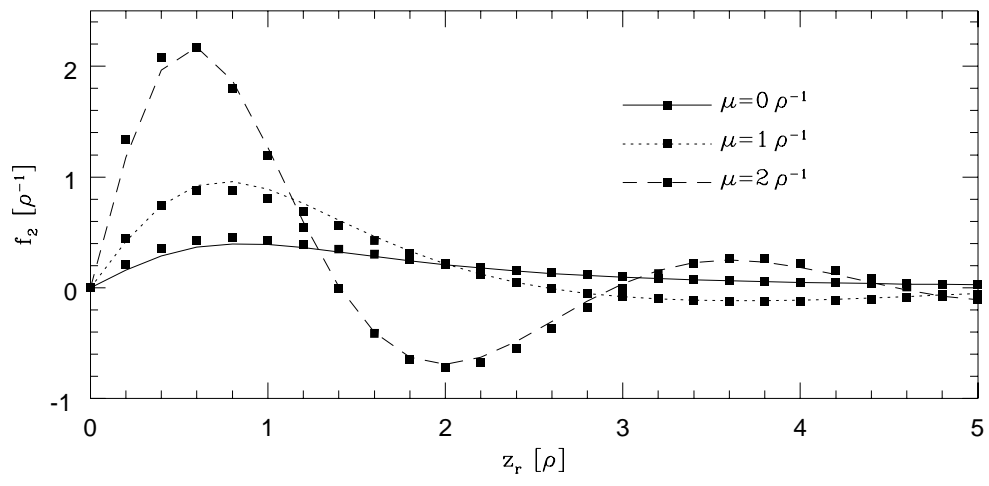
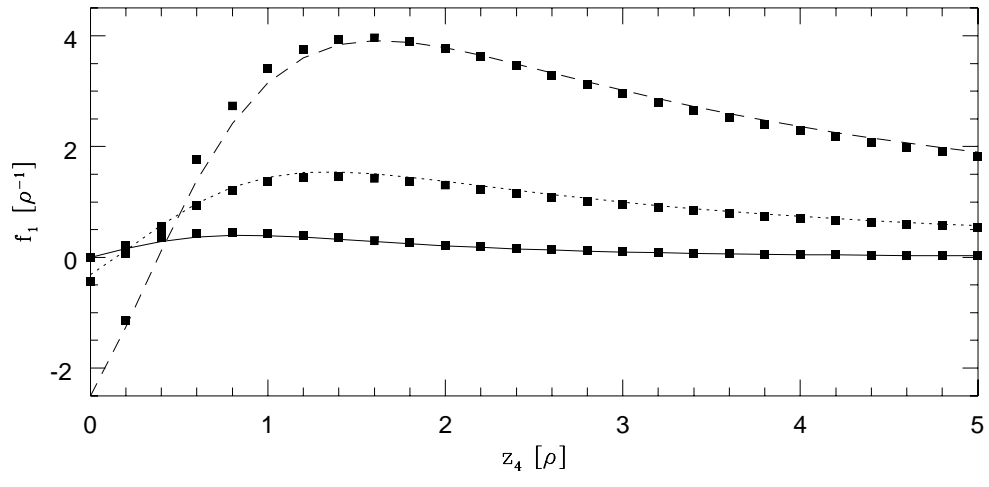


FIG. 1.

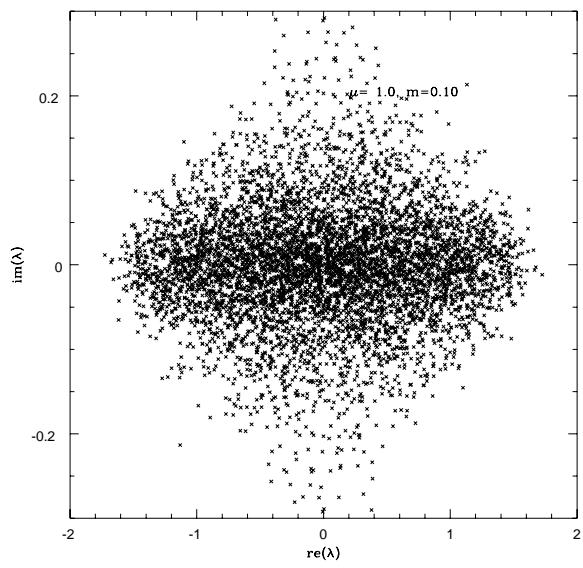
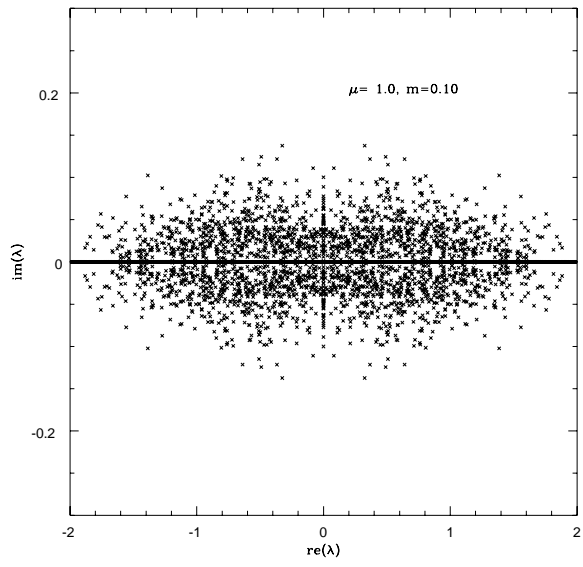


FIG. 2.

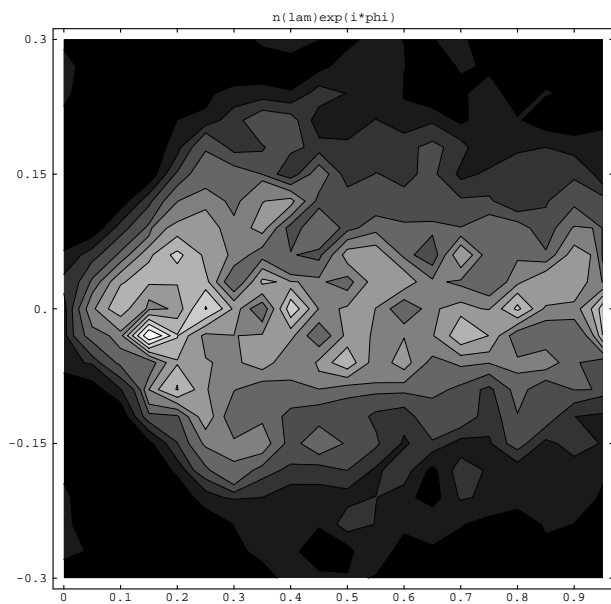
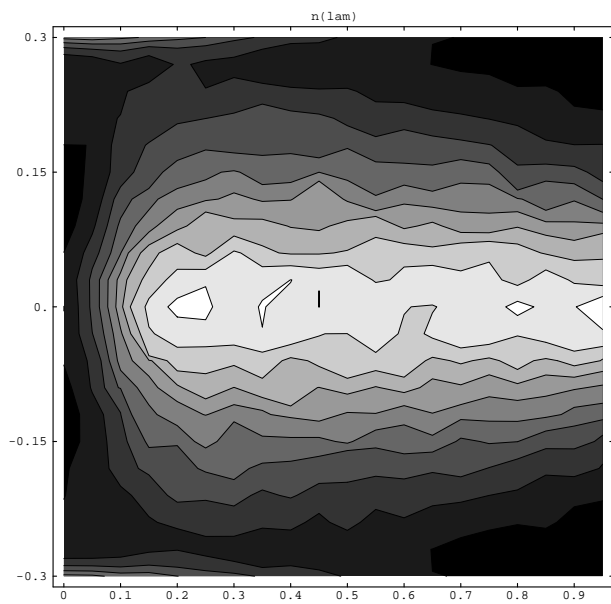


FIG. 3.

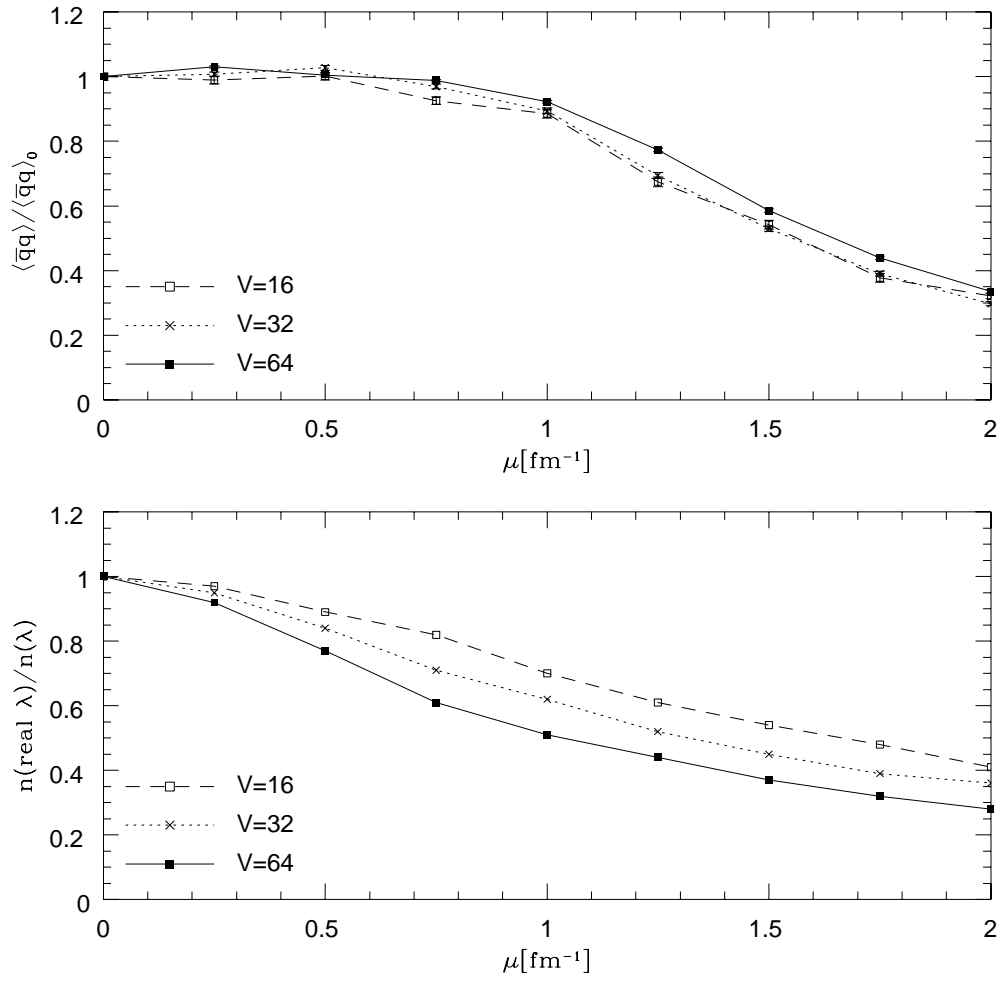


FIG. 4.

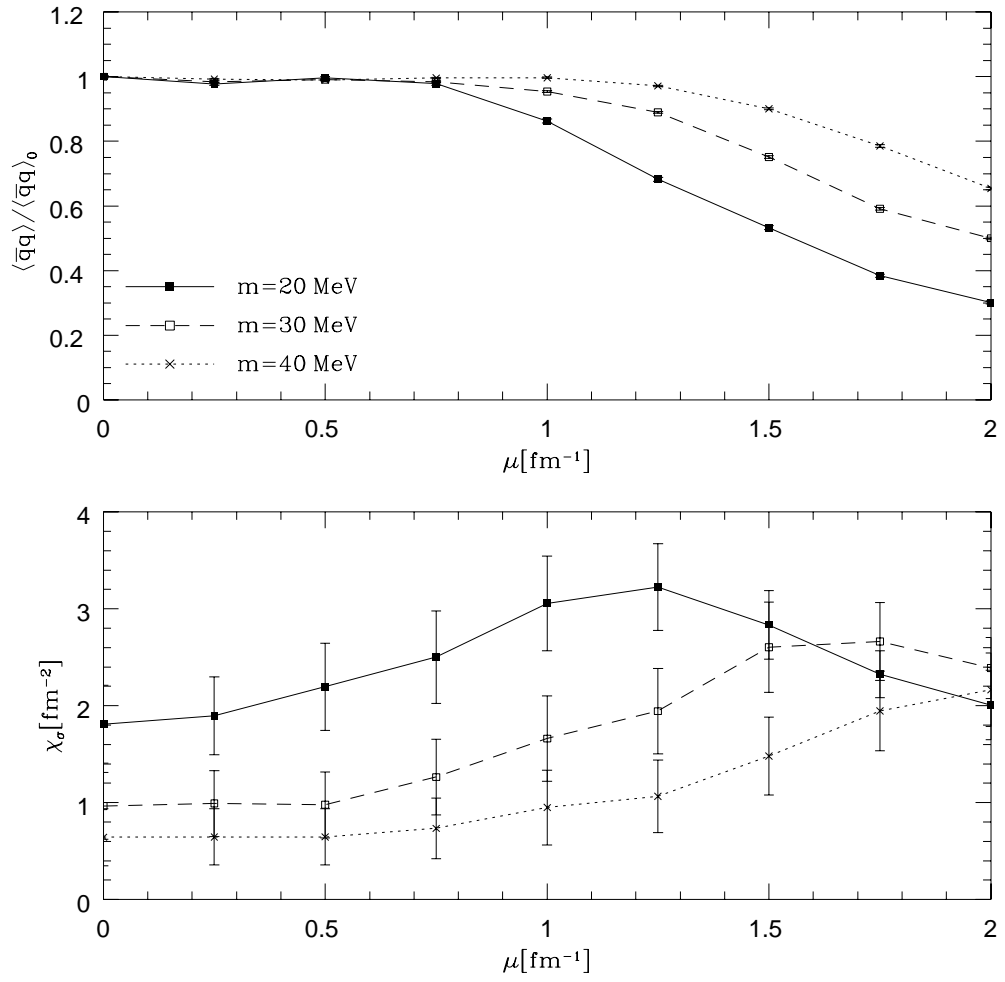


FIG. 5.

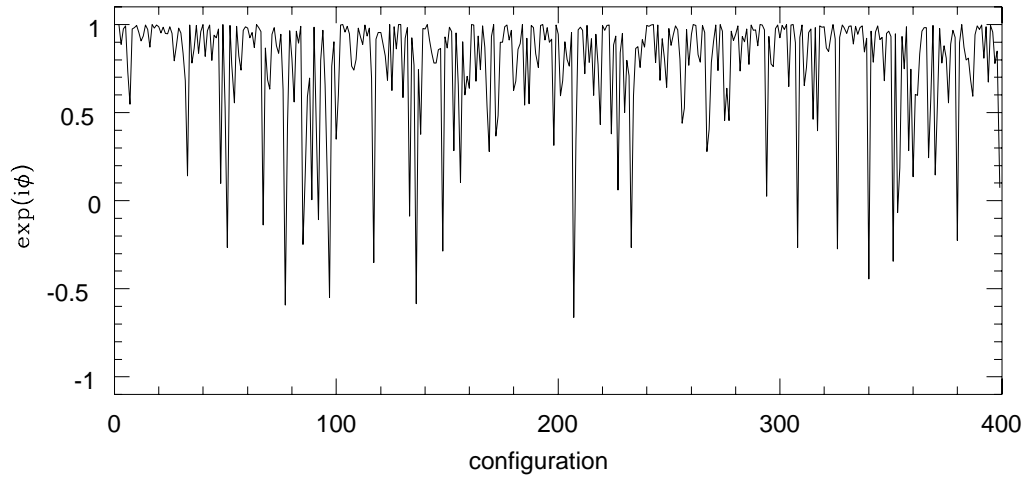
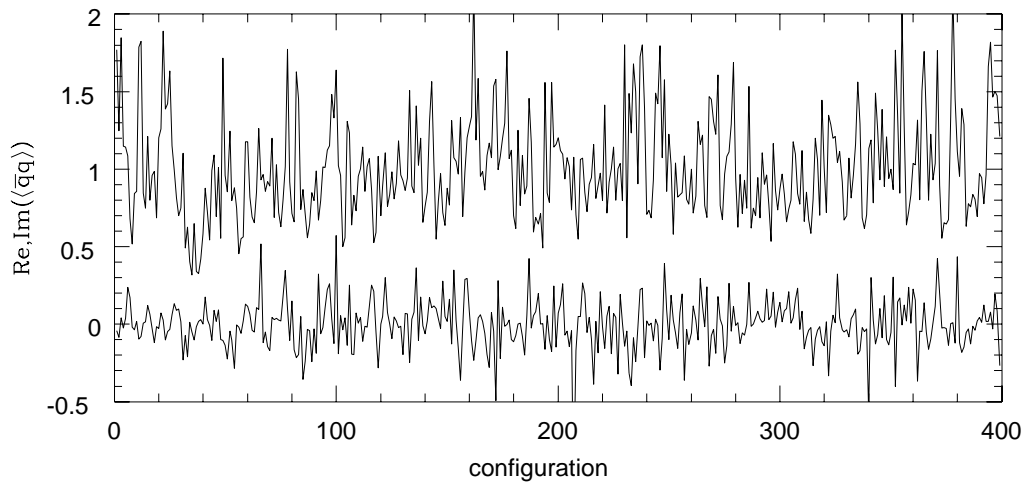


FIG. 6.

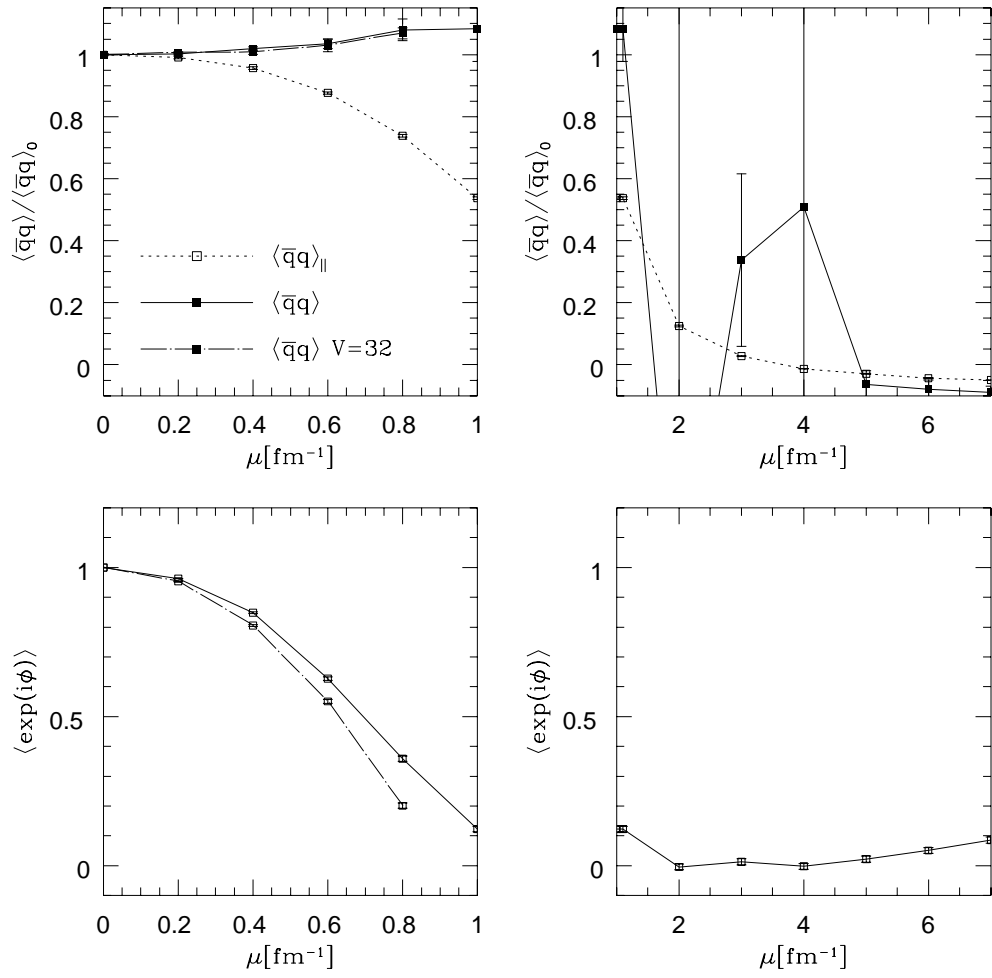


FIG. 7.

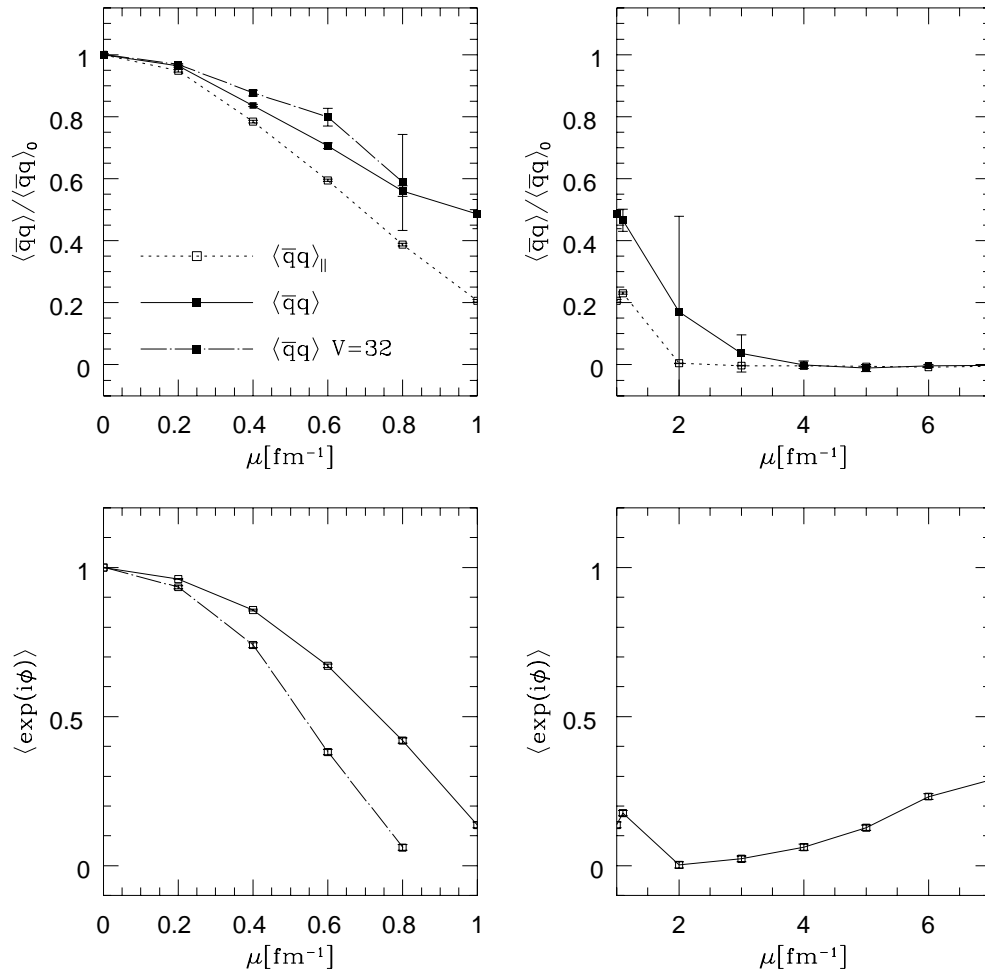


FIG. 8.

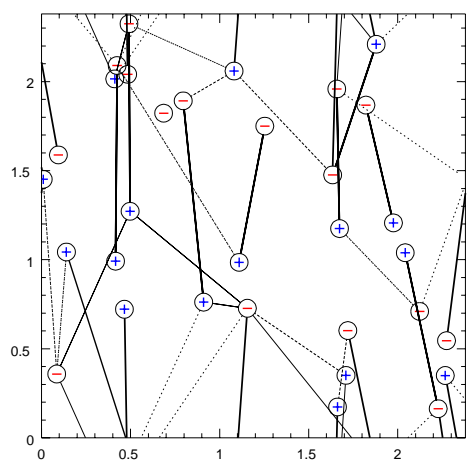
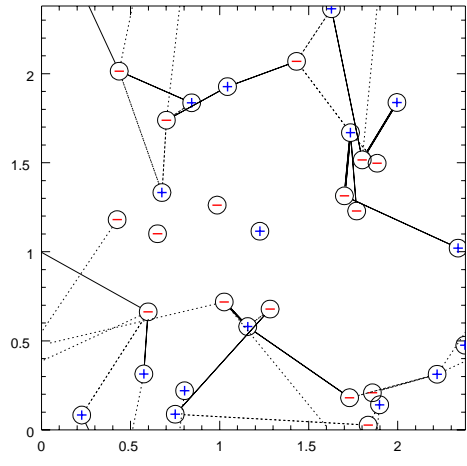


FIG. 9.

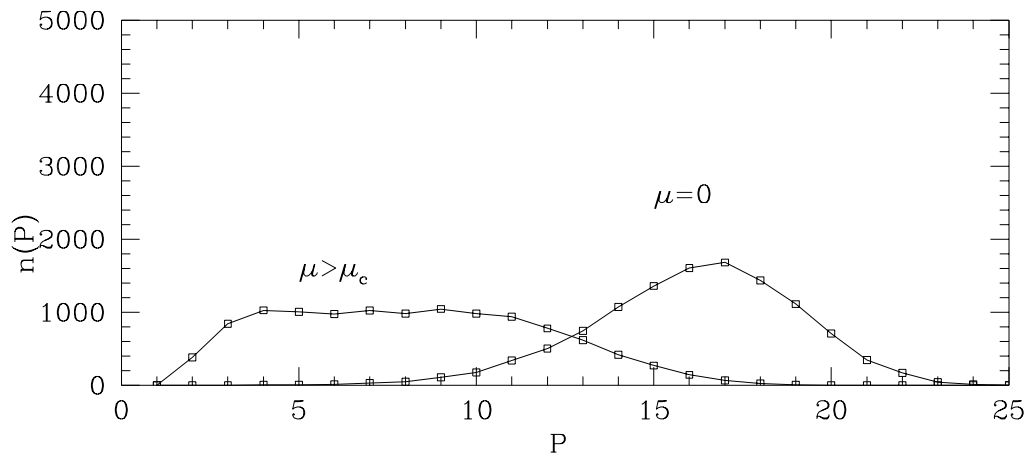
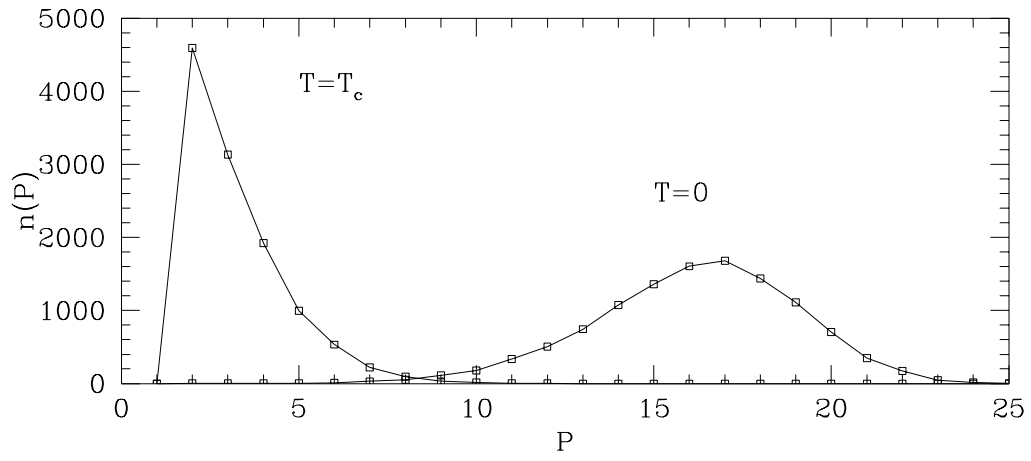


FIG. 10.